Charge-transfer host–guest complexes based on pillar[n]arenes and quinonoid compounds for near-infrared photothermal conversion

Aopu Wang[a], Xueru Zhao[a], Hui Zhang[a], Yanjun Ding[b], Min Xue[c] and Li Shao[a]*

[a]. School of Materials Science and Engineering, Zhejiang Sci-Tech University, Hangzhou, 310018, P. R. China. Email: lishao@zstu.edu.cn

[b]. School of Materials Science and Engineering, Anhui University, Hefei 230601, P. R. China

[c]. Department of Physics, Zhejiang Sci-Tech University, Hangzhou, 310018, P. R. China.

Supplementary Information (25 pages)

1. Materials and methods

All reagents were commercially available and used as supplied without further purification. Solvents were either employed as purchased or dried according to procedures described in the literature. Compounds **EtP5** and **EtP6** were synthesized according to previous literature.[1, 2] NMR spectra were recorded with a Bruker Avance DMX 400 spectrophotometer or a Bruker Avance DMX 500 spectrophotometer with the deuterated solvent as the lock and the residual solvent or TMS as the internal reference. UV-vis spectra were taken on a Persee TU-1901 UV-vis spectrophotometer. The fluorescence experiments were conducted on a RF-6000 spectrofluorophotometer (Shimadzu Corporation, Japan). The crystal data were collected on an Oxford Diffraction Xcalibur Atlas Gemini Ultra instrument. UV-Vis diffuse reflectance spectrum were taken on a Persee Shimadzu UV-2600 UV-vis spectrophotometer. Sample temperature measured under laser irradiation using Fotric 325. Potential map calculation is performed using Materials Studio packages. The theoretical calculations are carried out using the Gaussian 16 software packages.

2. Host–guest investigation of pillar[n]arene and guests

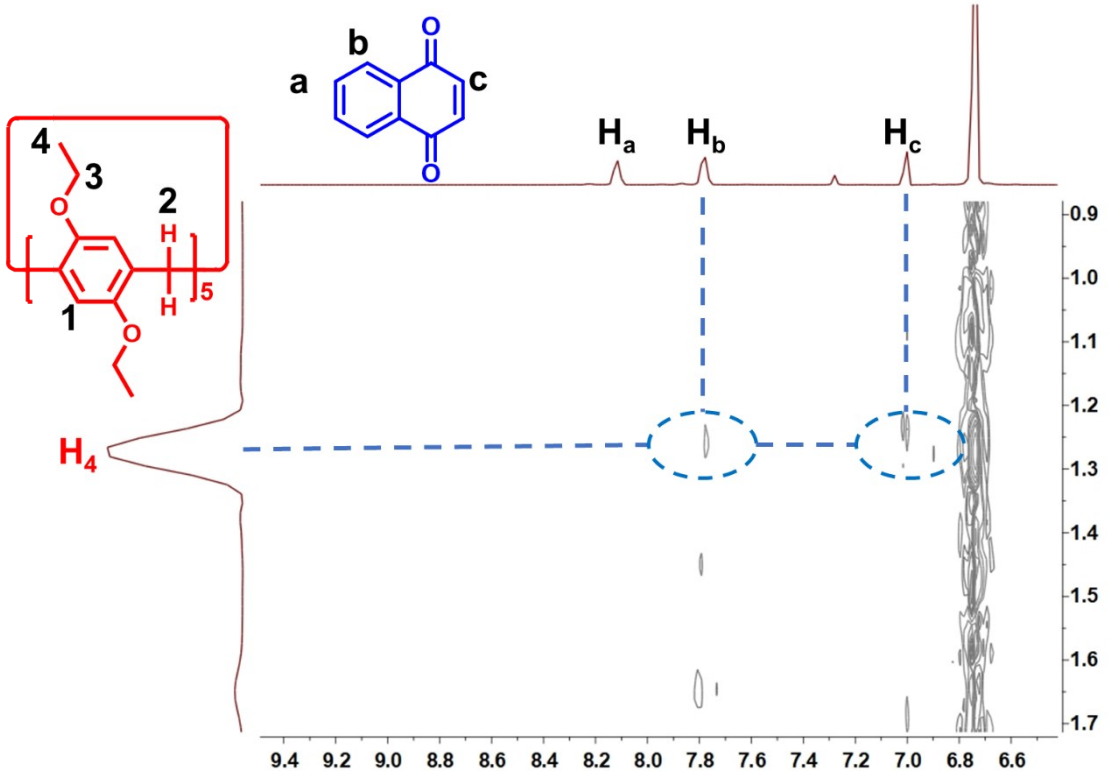

Figure S1. Partial NOESY NMR spectrum (500 MHz, $CDCl_3$, 293 K): **G1** (10.00 mM) and **EtP5** (10.00 mM).

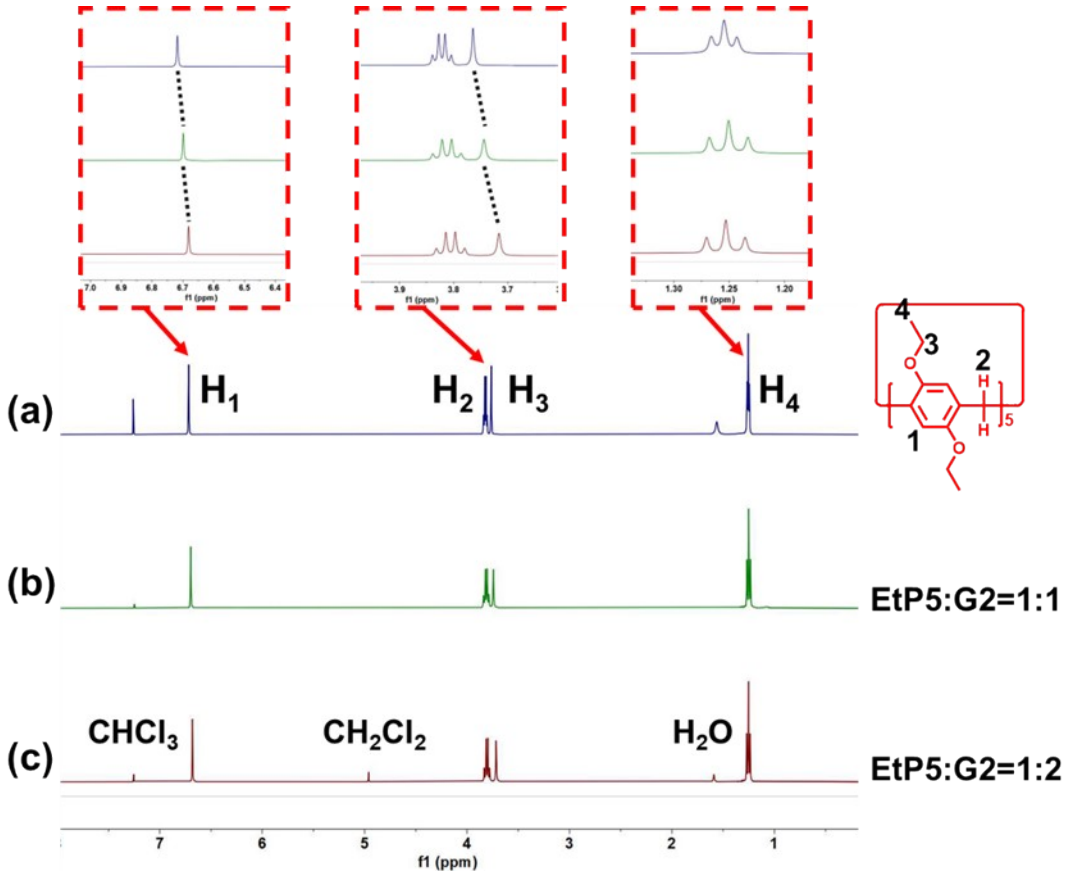

Figure S2. Partial ^{1}H NMR spectra (400 MHz, CDCl3, 293 K): (a) **EtP5**; (b) a mixture of **EtP5** and **G2** (1 : 1); (c) a mixture of **G2** and **EtP5** (1 : 2).

3. Stoichiometry and association constant determination for the host–guest complexes

To determine the association constant for the complexation between **EtP5**/**EtP6** and **G1**, **G2**, **G3**, fluorescence titration experiments were done with solutions which had a constant concentration of pillar[*n*]arenes and varying concentrations of guests. The stoichiometry was obtained by molar ratio plot. The association constant (K_a) was determined by a non-linear curve-fitting method.

Among them, the host−guest complexation with 1:1 stoichiometry was fitted by Eq. S1:

$$\Delta F = (\Delta F_\infty/[H]_0)\ (0.5[G] + 0.5([H]_0 + 1/K_a) - (0.5\ ([G]^2 + (2[G](1/K_a - [G])) + (1/K_a + [G])^2)^{0.5})) \qquad \text{Eq. S1}$$

where ΔF is the fluorescence intensity changes, ΔF_∞ is the fluorescence intensity change when pillar[*n*]arenes is completely complexed, [G] is the concentration of guests, and $[H]_0$ is the fixed initial concentration of pillar[*n*]arenes.

The host−guest complexation with 1:2 stoichiometry was fitted by Eq. S2:

$$\Delta F = (\Delta F_{HG} K_1[G] + \Delta F_{HG2} K_1 K_2 [G]^2) / (1 + K_1[G] + K_1 K_2 [G]^2) \qquad \text{Eq. S2}$$

where ΔF is the fluorescent change, ΔF_{HG} is the fluorescent change when guest is complexed by 1 equiv. pillararene, ΔF_{HG2} is the fluorescent change when guest is completely complexed by pillararene. [G] is the varying concentration of guest.

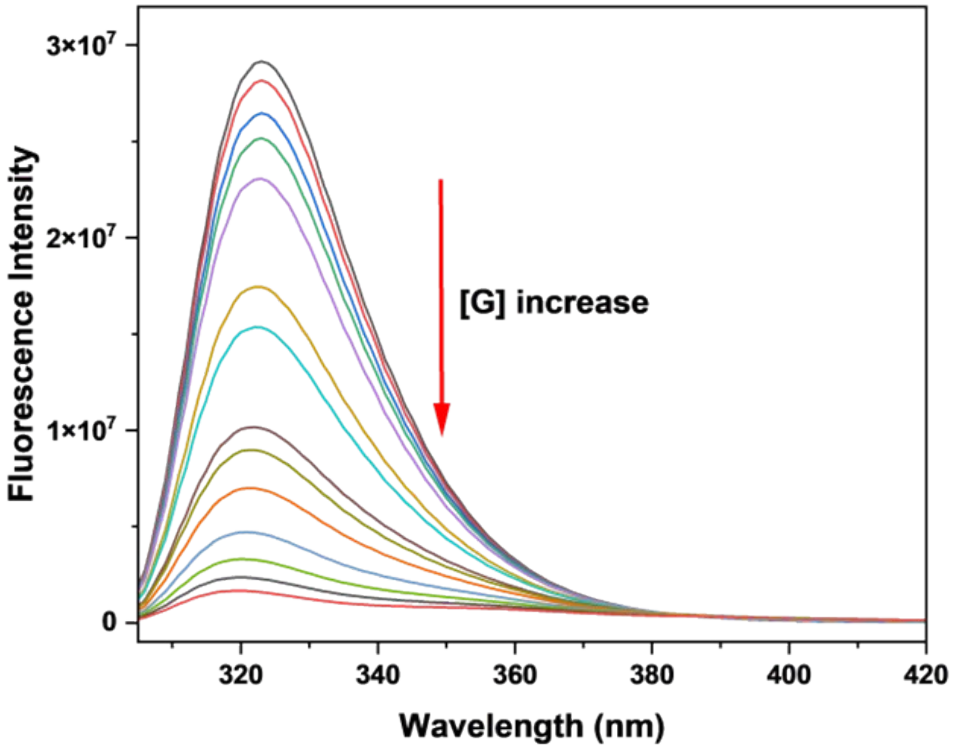

Figure S3. Fluorescence spectra of **EtP5** at a concentration of 0.1 mM in THF at room temperature upon addition of different concentrations of **G1** (0–0.7 mM).

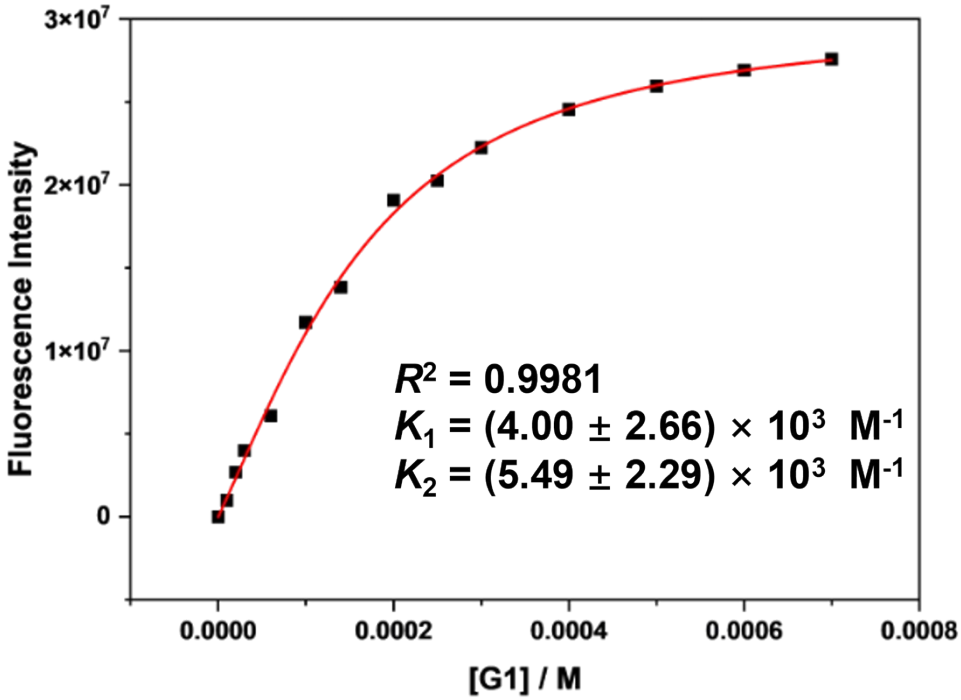

Figure S4. The fluorescence intensity changes of **EtP5** upon addition of **G1**. The red solid line was obtained from the non-linear curve-fitting method based on the Eq. S2.

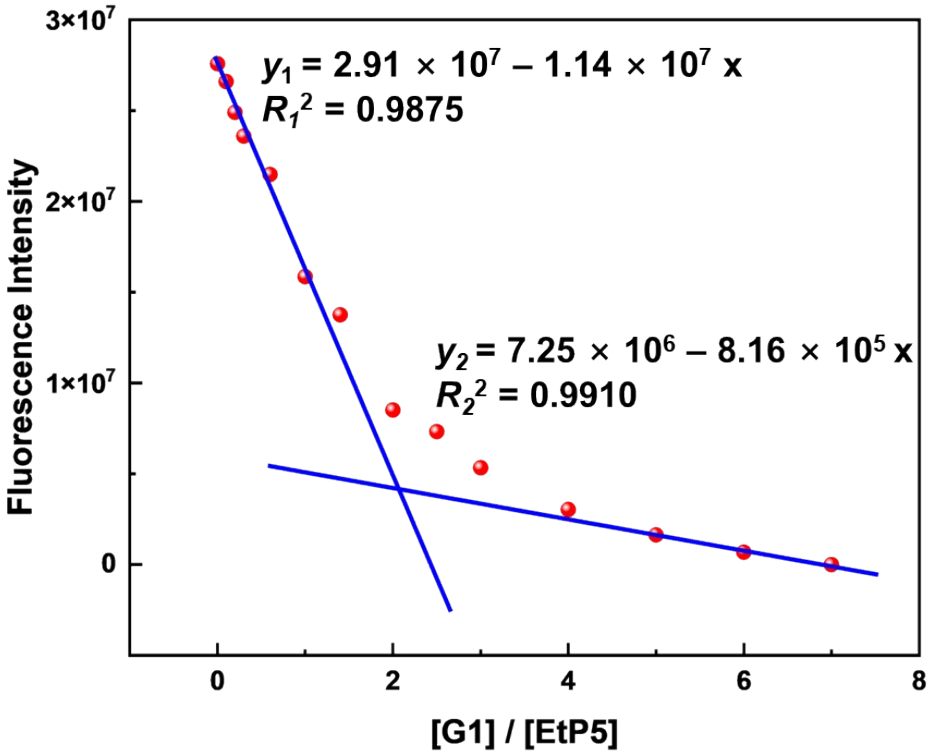

Figure S5. Molar ratio plot for the complexation between **G1** and **EtP5** in THF, indicating a 2:1 binding stoichiometry.

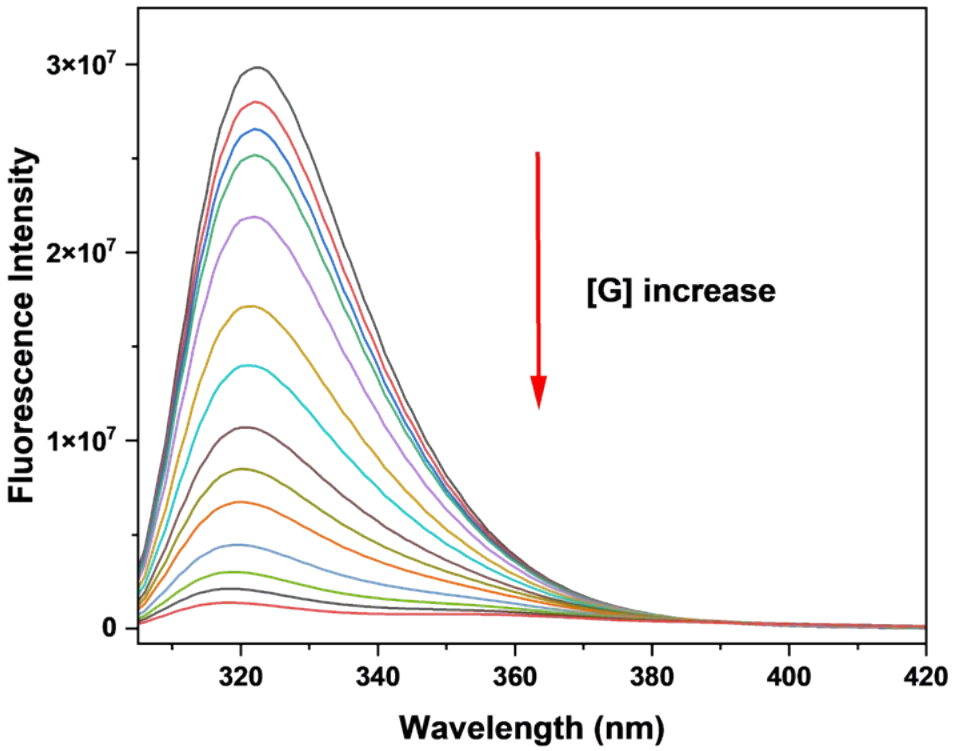

Figure S6. Fluorescence spectra of **EtP6** at a concentration of 0.1 mM in THF at room temperature upon addition of different concentrations of **G1** (0–0.7 mM).

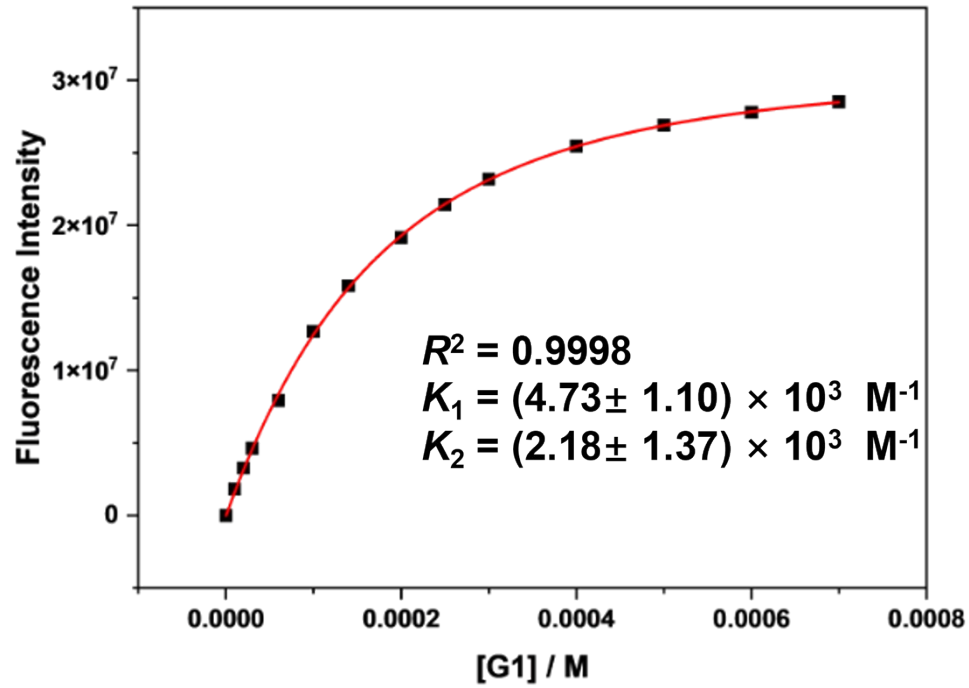

Figure S7. The fluorescence intensity changes of **EtP6** upon addition of **G1**. The red solid line was obtained from the non-linear curve-fitting method based on the Eq. S2.

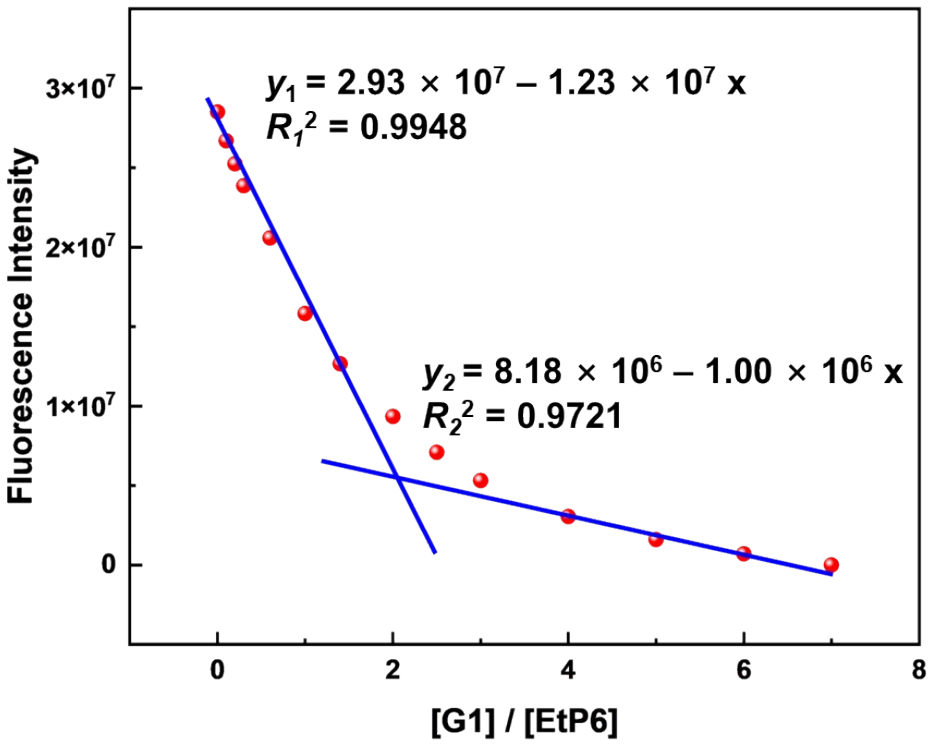

Figure S8. Molar ratio plot for the complexation between **G1** and **EtP6** in THF, indicating a 2:1 binding stoichiometry.

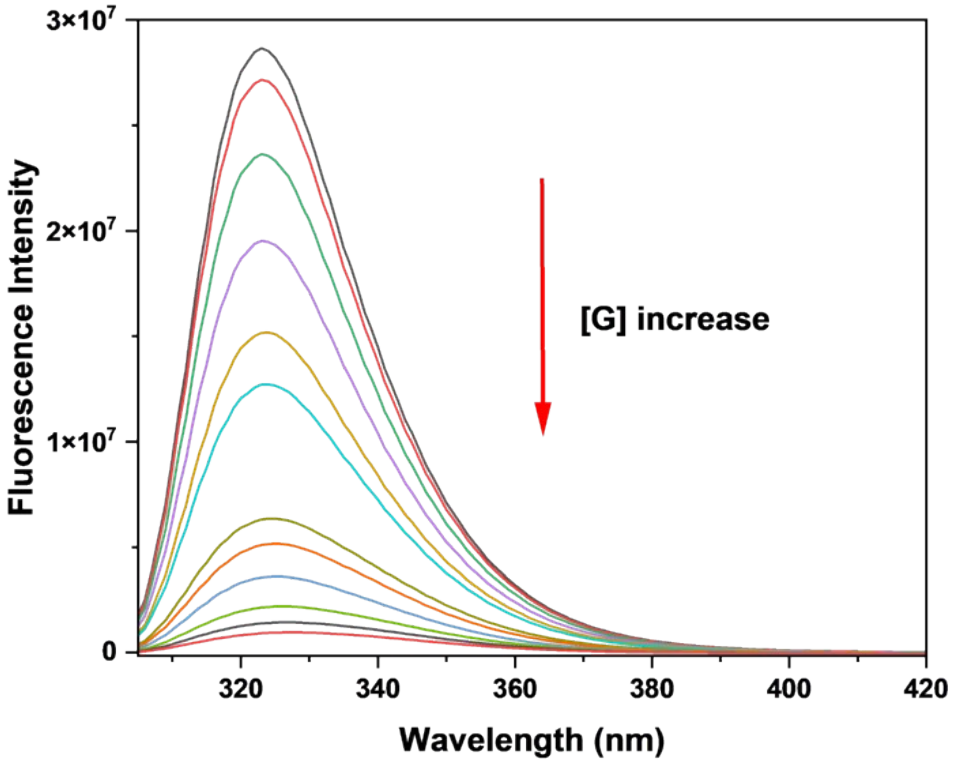

Figure S9. Fluorescence spectra of **EtP5** at a concentration of 0.1 mM in THF at room temperature upon addition of different concentrations of **G2** (0–0.7 mM).

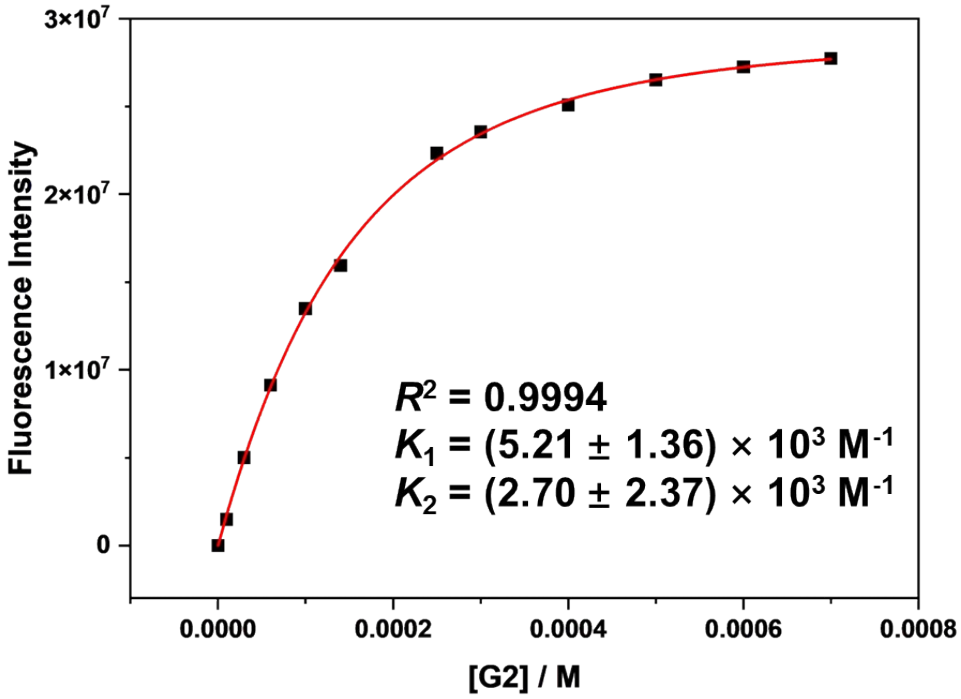

Figure S10. The fluorescence intensity changes of **EtP5** upon addition of **G2**. The red solid line was obtained from the non-linear curve-fitting method based on the Eq. S2.

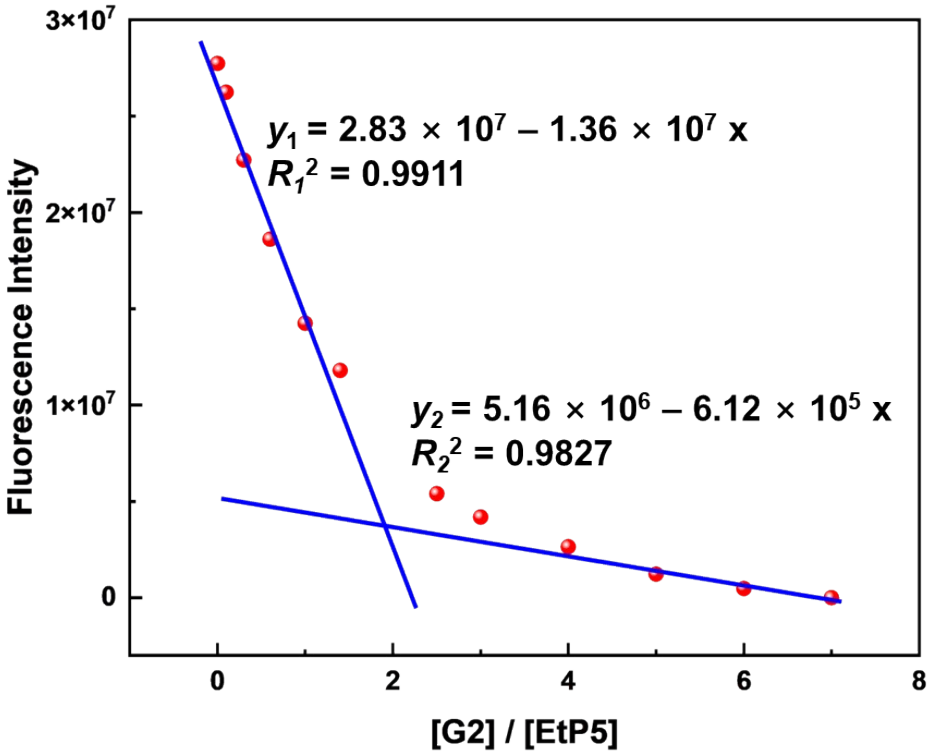

Figure S11. Molar ratio plot for the complexation between **G2** and **EtP5** in THF, indicating a 2:1 binding stoichiometry.

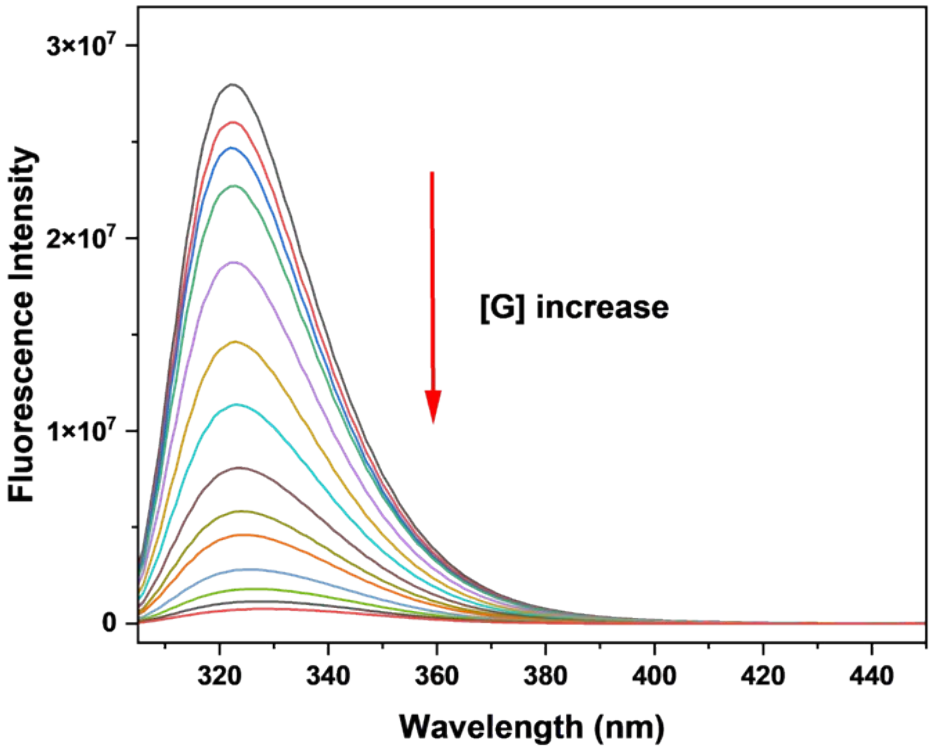

Figure S12. Fluorescence spectra of **EtP6** at a concentration of 0.1 mM in THF at room temperature upon addition of different concentrations of **G2** (0–0.7 mM).

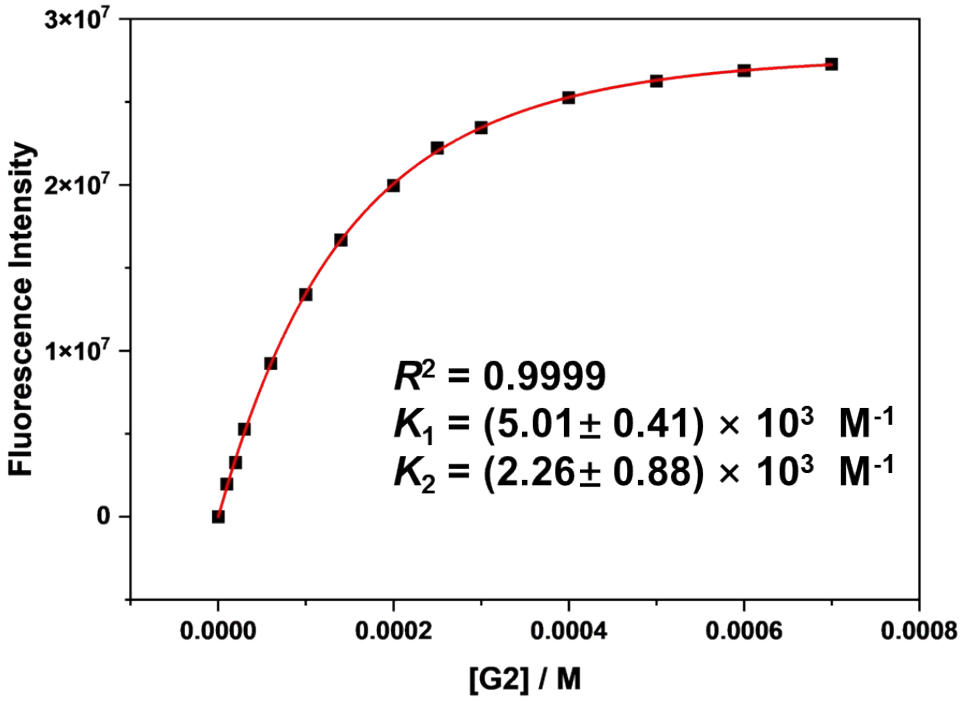

Figure S13. The fluorescence intensity changes of **EtP6** upon addition of **G2**. The red solid line was obtained from the non-linear curve-fitting method based on the Eq. S2.

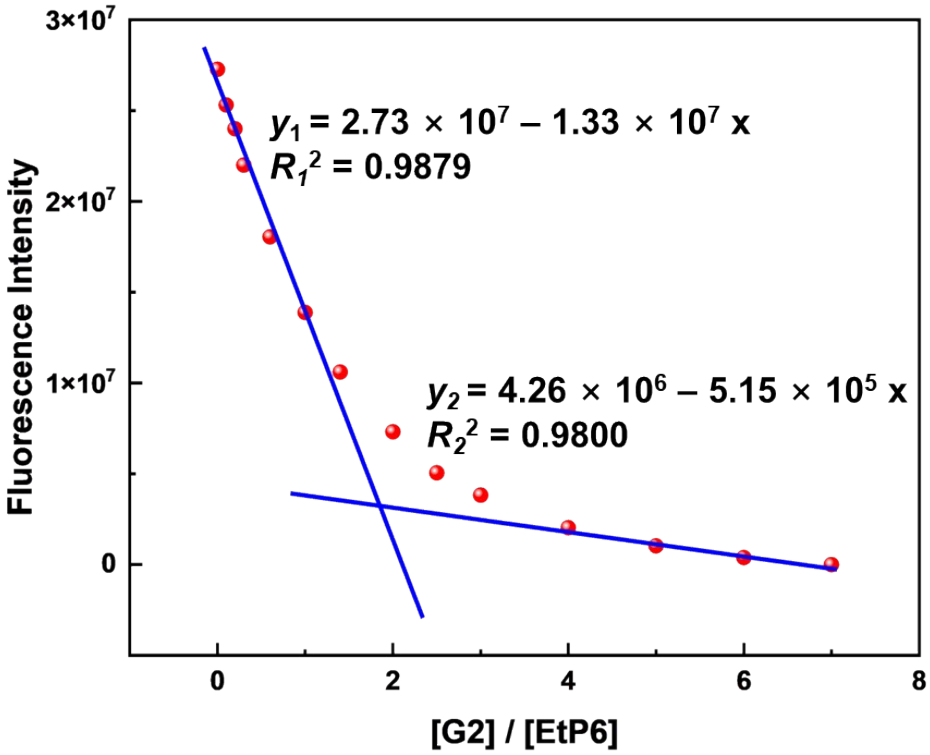

Figure S14. Molar ratio plot for the complexation between **G2** and **EtP6** in THF, indicating a 2:1 binding stoichiometry.

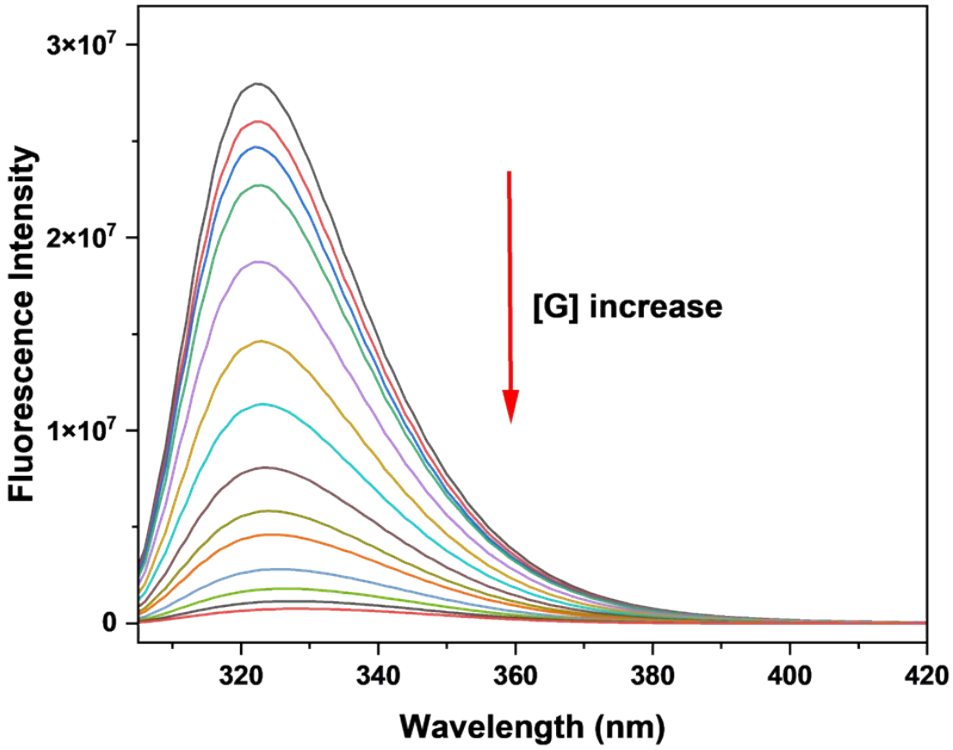

Figure S15. Fluorescence spectra of **EtP5** at a concentration of 0.1 mM in THF at room temperature upon addition of different concentrations of **G3** (0–0.7 mM).

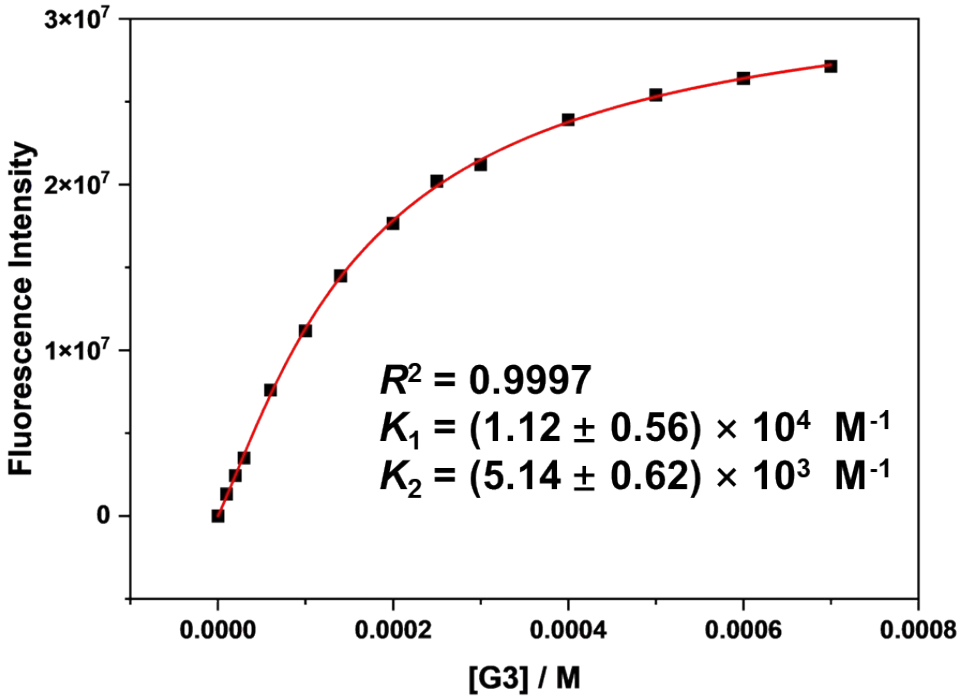

Figure S16. The fluorescence intensity changes of **EtP5** upon addition of **G3**. The red solid line was obtained from the non-linear curve-fitting method based on the Eq. S2.

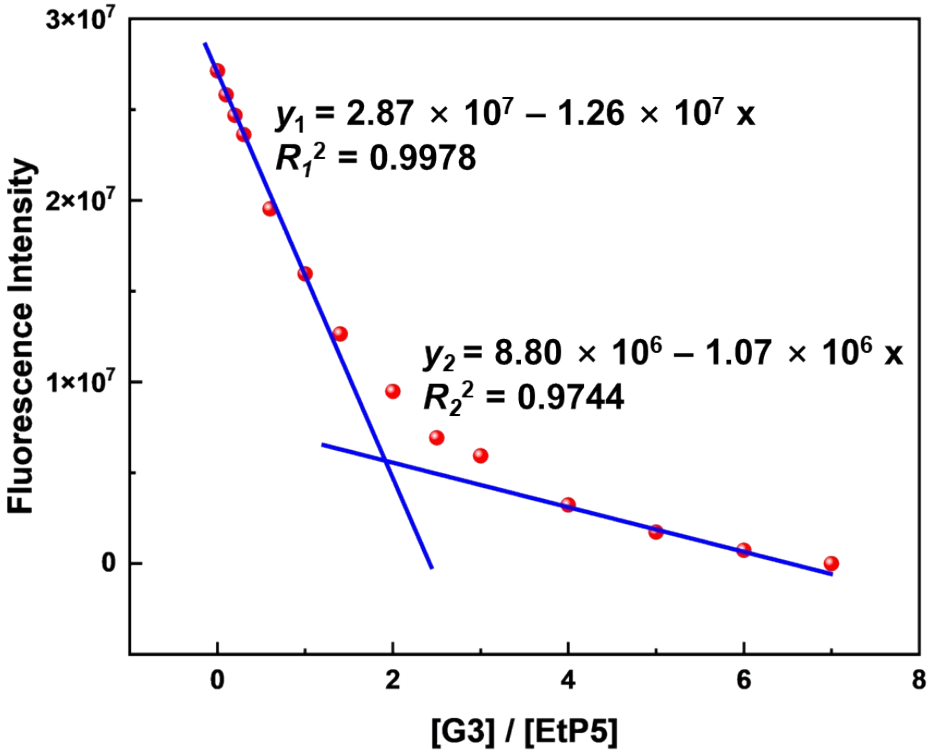

Figure S17. Molar ratio plot for the complexation between **G3** and **EtP5** in THF, indicating a 2:1 binding stoichiometry.

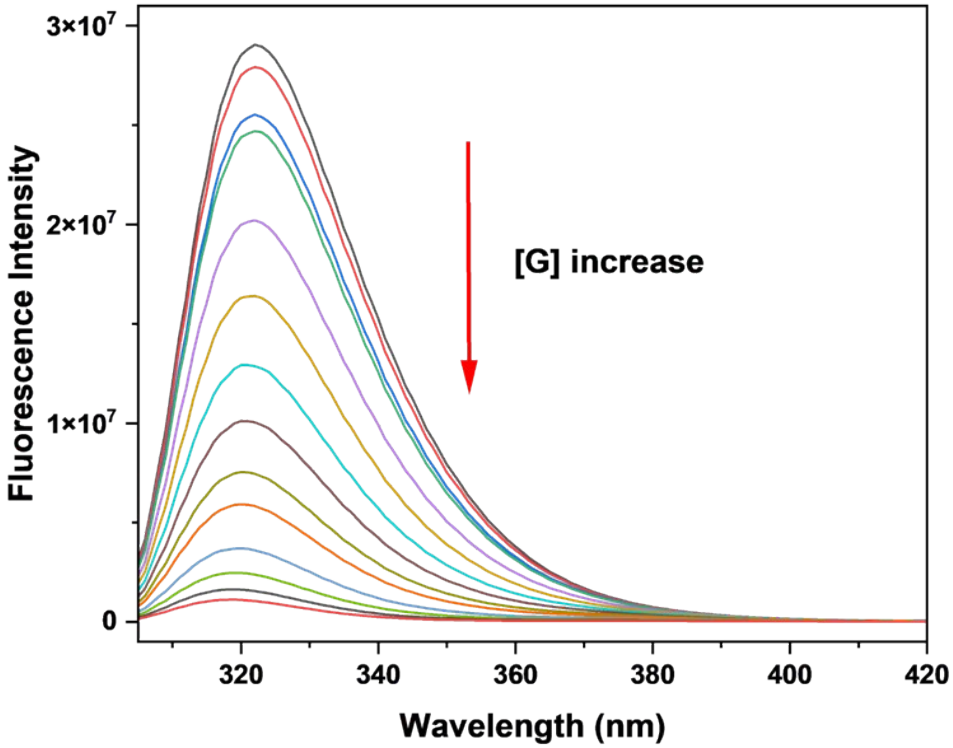

Figure S18. Fluorescence spectra of **EtP6** at a concentration of 0.1 mM in THF at room temperature upon addition of different concentrations of **G3** (0–0.7 mM).

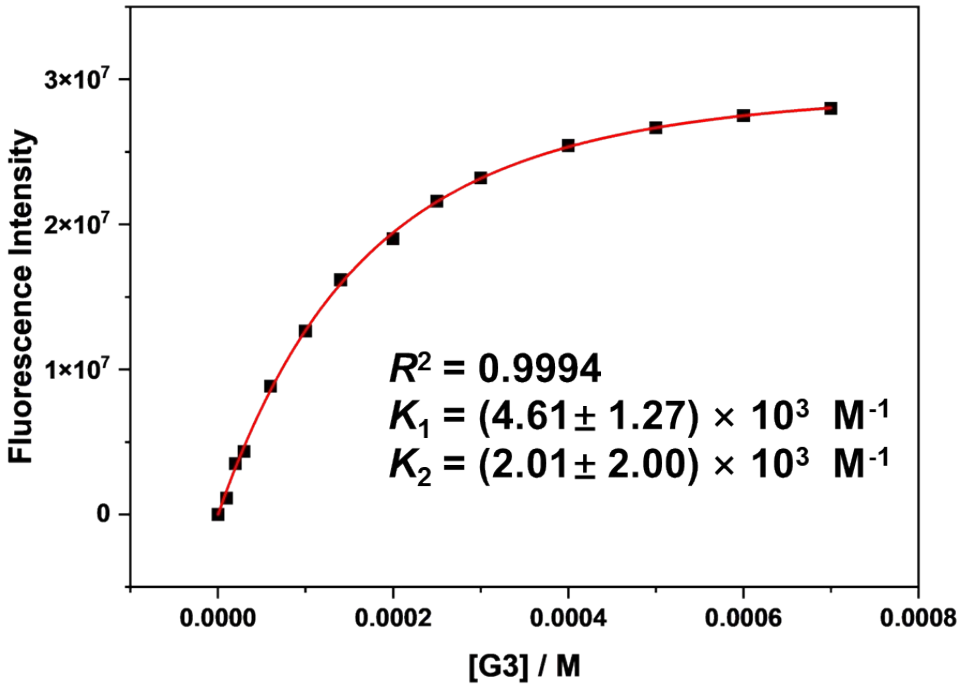

Figure S19. The fluorescence intensity changes of **EtP6** upon addition of **G3**. The red solid line was obtained from the non-linear curve-fitting method based on the Eq. S2.

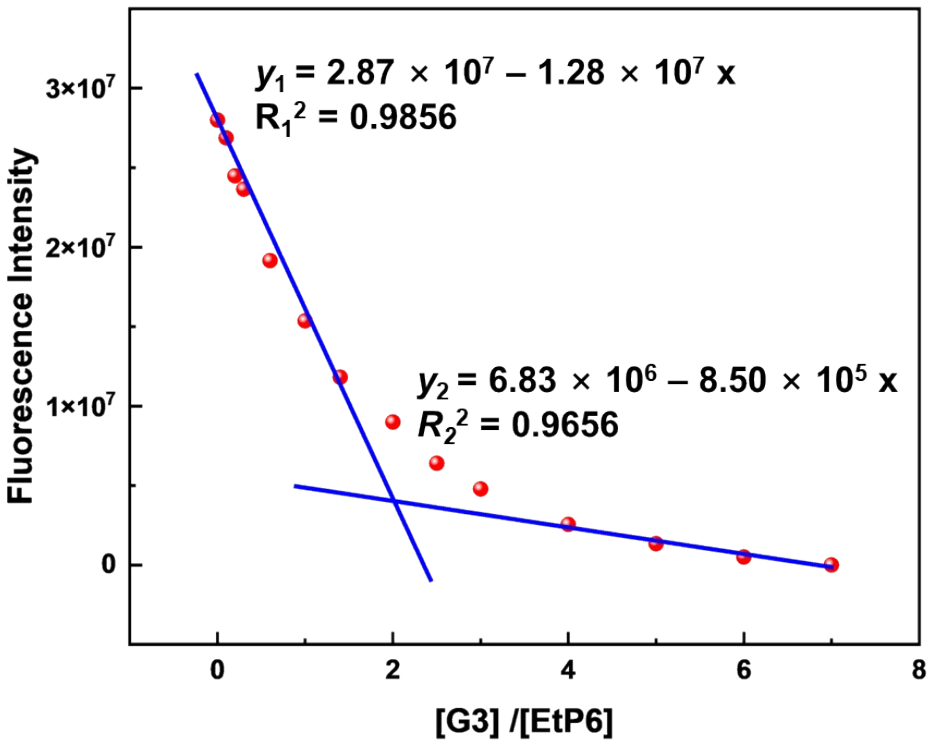

Figure S20. Molar ratio plot for the complexation between **G3** and **EtP6** in THF, indicating a 2:1 binding stoichiometry.

4.UV-vis spectra and macroscopic color changes before and after host–guest complex formation

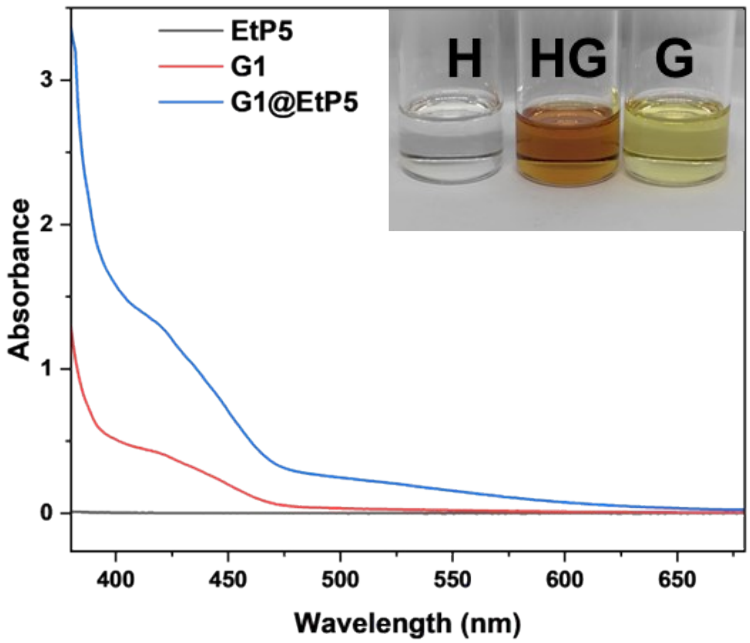

Figure S21. UV-vis spectra ($CHCl_3$) of (**H**) **EtP5** (20.0 mM), (**G**) **G1** (20.0 mM), (**HG**) **EtP5** (20.0 mM) and **G1** (40.0 mM), and macroscopic color changes.

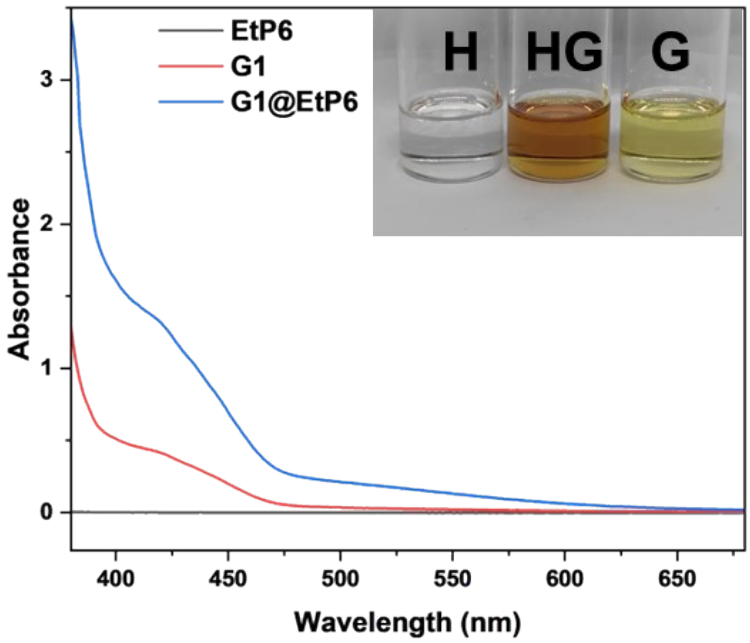

Figure S22. UV-vis spectra ($CHCl_3$) of (**H**) **EtP6** (20.0 mM), (**G**) **G1** (20.0 mM), (**HG**) **EtP6** (20.0 mM) and **G1** (40.0 mM), and macroscopic color changes.

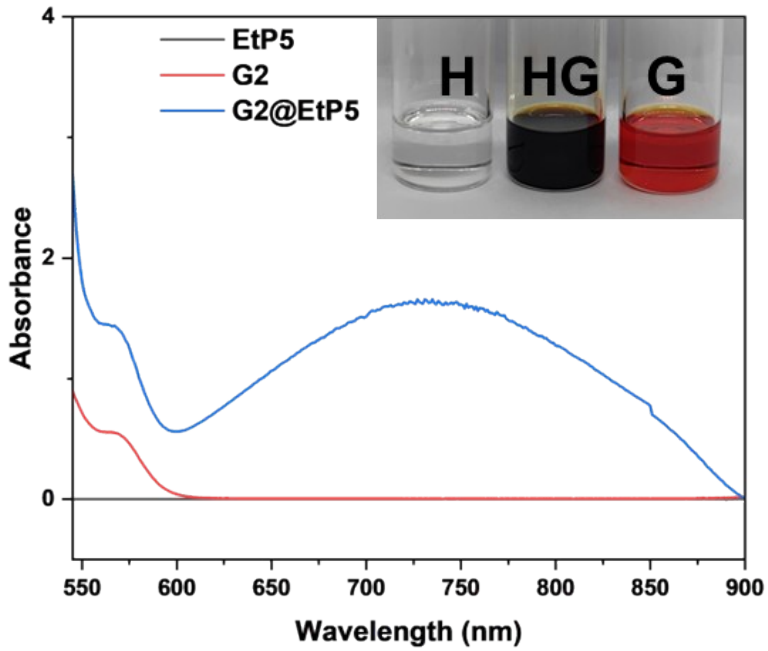

Figure S23. UV-vis spectra ($CHCl_3$) of (**H**) **EtP5** (20.0 mM), (**G**) **G2** (20.0 mM), (**HG**) **EtP5** (20.0 mM) and **G2** (40.0 mM), and macroscopic color changes.

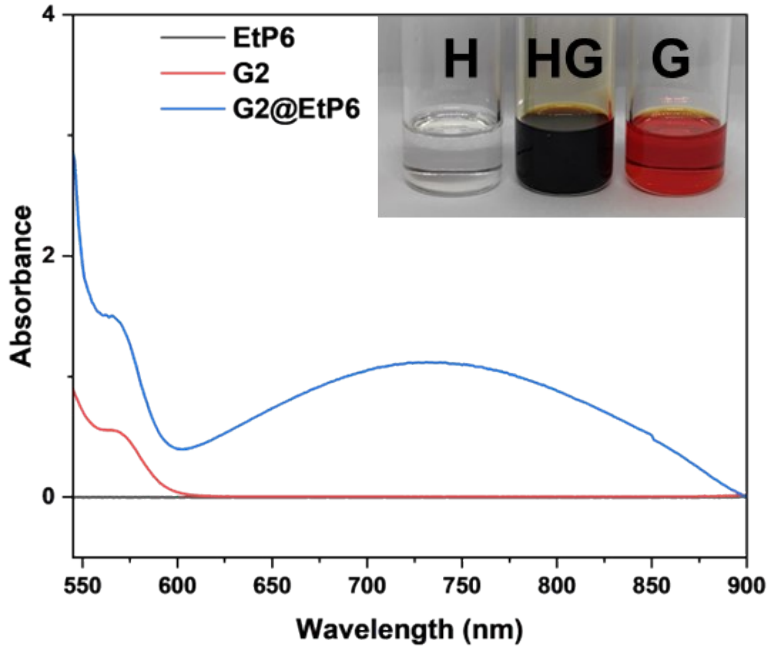

Figure S24. UV-vis spectra ($CHCl_3$) of (**H**) **EtP6** (20.0 mM), (G) **G2** (20.0 mM), (**HG**) **EtP6** (20.0 mM) and **G2** (40.0 mM), and macroscopic color changes.

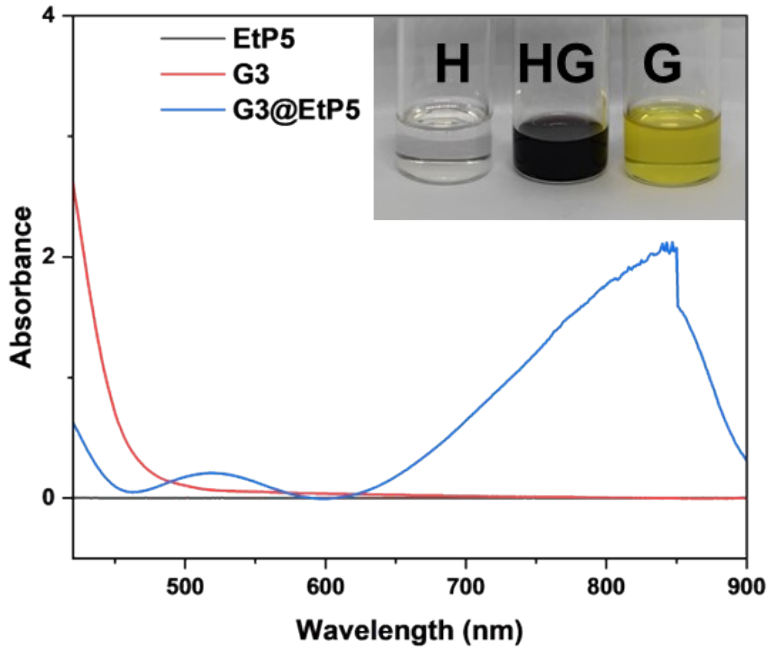

Figure S25. UV-vis spectra ($CHCl_3$) of (**H**) **EtP5** (20.0 mM), (**G**) **G2** (20.0 mM), (**HG**) **EtP5** (4.0 mM) and **G2** (8.0 mM), and macroscopic color changes.

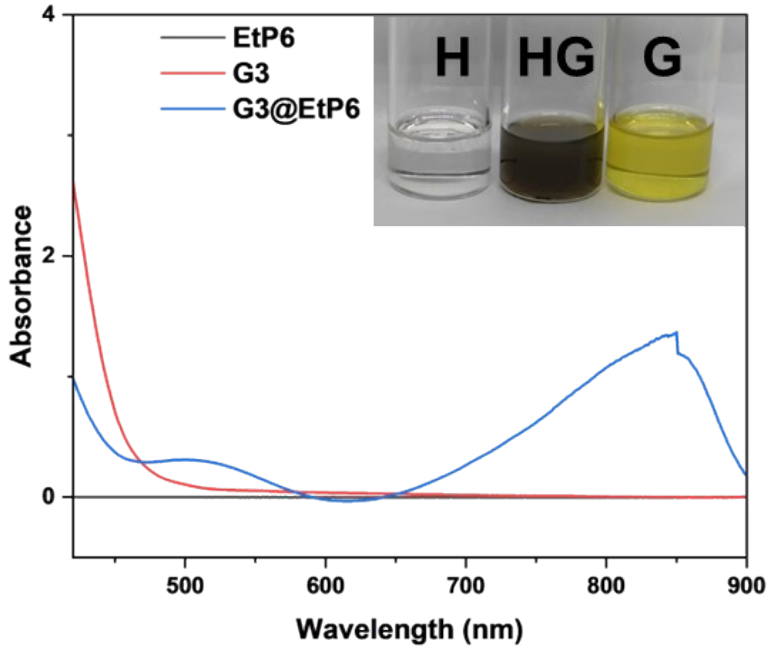

Figure S26. UV-vis spectra ($CHCl_3$) of (**H**) **EtP6** (20.0 mM), (**G**) **G2** (20.0 mM), (**HG**) **EtP6** (5.0 mM) and **G2** (10.0 mM), and macroscopic color changes.

5. Molecular orbital diagrams.

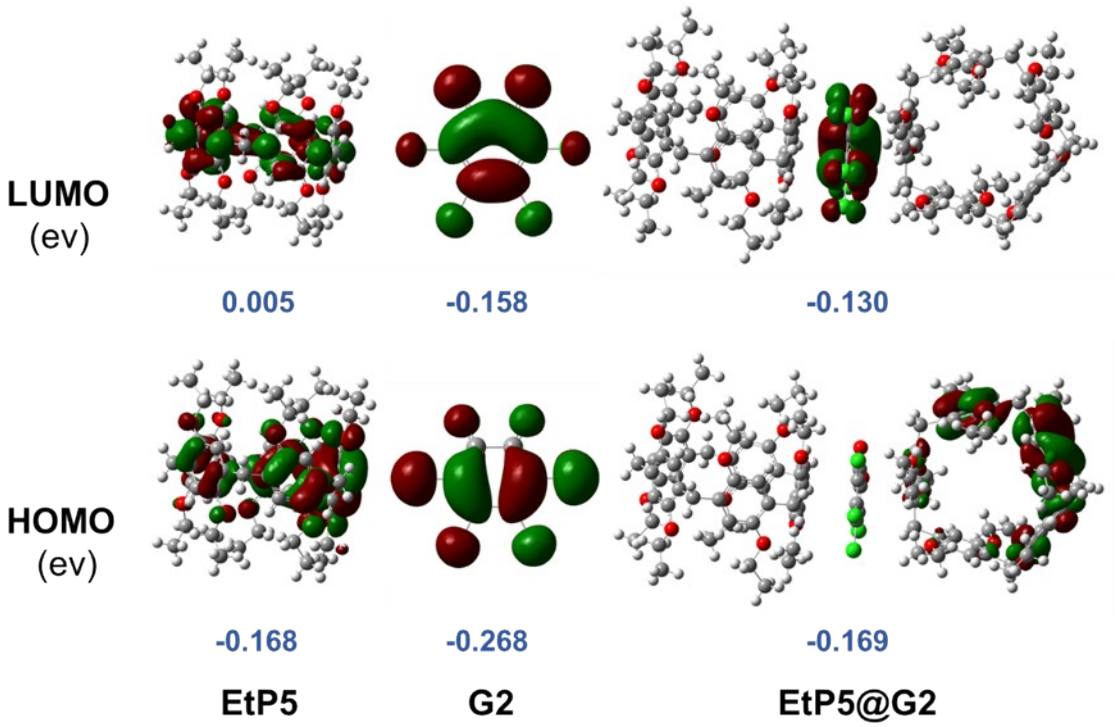

Figure S27. Molecular orbital (MO) diagrams of **EtP5**, **G2**, and **EtP5@G2**.

6. Calculation of photothermal conversion efficiencies

The calculation of photothermal conversion efficiency was determined according to previous methods [3]. Based on the total energy balance for this system:

$$\sum_i m_i C_{p,i} \frac{dT}{dt} = Q_s - Q_{loss}$$

Where m_i (0.4002g for **EtP5@G2**) and $C_{p,i}$（0.8 J/(g °C)）are the mass and heat capacity of system components (cocrystal samples and quartz glass), respectively. The mass of cocrystal samples is negligible with that of quartz glass, the heat capacity of quartz glass is therefore used for photothermal conversion efficiency of cocrystal samples. Q_s is the photothermal heat energy input by irradiating NIR laser to cocrystal samples, and Q_{loss} is thermal energy lost to the surroundings. When the temperature is maximum, the system is in balance.

$$Q_s = Q_{loss} = hS\Delta T_{max}$$

Where h is the heat transfer coefficient, S is the surface area of the container, ΔT_{max} is the maximum temperature change. The photothermal conversion efficiency η is calculated from the following equation:

$$\eta = \frac{hS\Delta T_{max}}{I(1 - 10^{-A_{808}})}$$

Where I is the laser power (1.0 W cm^{-2}) and A_{808} is the absorbance of the cocrystal samples at the wavelength of 808 nm (0.521 for **EtP5@G2**).

In order to obtain the hS, a dimensionless driving force temperature, θ is introduced as follows:

$$\theta = \frac{T - T_{surr}}{T_{max} - T_{surr}}$$

where T is the temperature of cocrystal samples, T_{max} is the maximum system temperature, and T_{surr} is the initial surrounding temperature.

The sample system time constant τ_s

$$\tau_s = \frac{\sum_i m_i C_{p,i}}{hS}$$

thus $$\frac{d\theta}{dt} = \frac{1}{\tau_s hS\Delta T_{max}} Q_S - \frac{\theta}{\tau_s}$$

when the laser is off, $Q_s = 0$, therefore $\frac{d\theta}{dt} = -\frac{\theta}{\tau_s}$, and $t = -\tau_s \ln \theta$

so hS could be calculated from the slope of cooling time vs $\ln \theta$. Therefore, the average τ_s is 114.87 s for **EtP5@G2** (Figure. S28). And the photothermal conversion efficiency η of **EtP5@G2** cocrystals is 16.76 ± 0.22%.

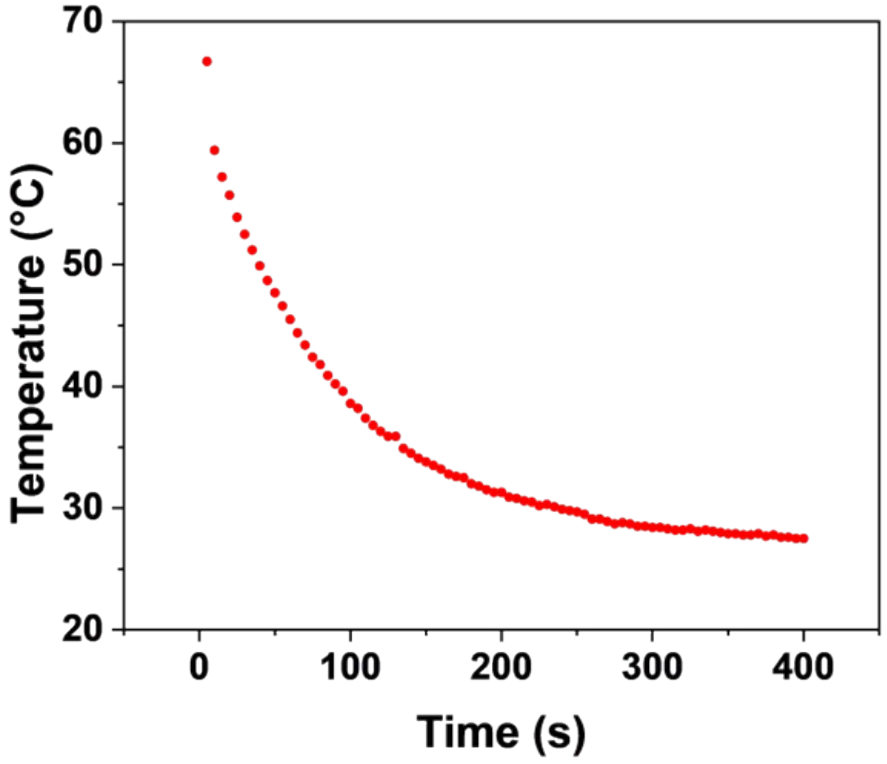

Figure. S28. Cooling curves of **EtP5@G2** cocrystal at 1.0 W cm^{-2}.

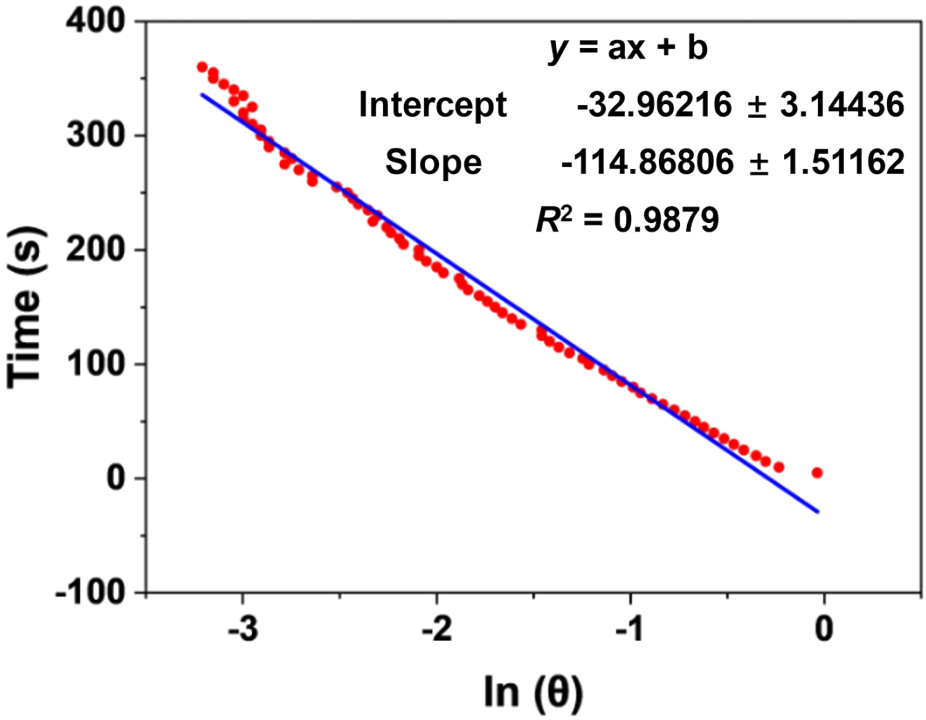

Figure. S29. Linear fitting of time vs Ln (θ).

7. References

[1]. S. Chao, Z. Shen, Y. Pei, Y. Lv, X. Chen, J. Ren, K. Yang and Z. Pei, *Chem. Commun.*, 2021, **57**, 7625-7628.

[2]. D. Cao, Y. Kou, J. Liang, Z. Chen, L. Wang and H. Meier, *Angew. Chem. Int. Ed.*, 2009, **48**, 9721-9723.

[3]. J. Xu, W. Chen, S. Li, Q. Chen, T. Wang, Y. Shi, S. Deng, M. Li, P. Wei and Z. Chen, *Chin. Chem. Lett.*, 2024, **35**, 109808.